Geophysical Research Letters

RESEARCH LETTER
10.1029/2021GL095504

Special Section:
Southern Ocean and Climate: Biogeochemical and Physical Fluxes and Processes

Investigating Predictability of DIC and SST in the Argentine Basin Through Wind Stress Perturbation Experiments

Stan Swierczek[1], Matthew R. Mazloff[2], and Joellen L. Russell[3]

[1]American Society for Engineering Education, Washington, DC, USA, [2]Scripps Institution of Oceanography, La Jolla, CA, USA, [3]Department of Geosciences, University of Arizona, Tucson, AZ, USA

Abstract The confluence of the Malvinas and Brazil currents over the Argentine Basin give the region chaotic dynamics and severely limit potential predictability. To probe the forecast horizon for ocean surface quantities of temperature and carbon, we construct regional models of the Argentine Basin with biogeochemistry at 1/3° and 1/12° resolution and design a series of experiments. We add positive and negative zonal wind stress anomalies over small and large areas during a short period in different model runs. We calculate the response of the surface temperature and DIC. The 1/3° model maintains predictability for up to 45 days, while the 1/12° model has a shorter window of about two weeks. However, the 1/3° model response is only consistent with the 1/12° model for about 8 days calling into question the potential predictive skill of the coarser model at longer lead times.

Plain Language Summary The Argentine Basin is a turbulent region in the Southern Ocean that is not well understood. We want to determine how well we can make forecasts of the region given some level of error in our starting point, and additionally investigate the dependence of model resolution on our ability to forecast. We design a series of numerical experiments where we make a change in the winds at the start of the model run and quantify how the heat and carbon in the surface ocean change compared to model runs without changing the winds. These differences are measured as time progresses. We determine that in the coarser resolution models, the differences decay for up to 45 days before increasing, whereas in the finer resolution model the differences decay for two weeks before increasing. This gives us a time frame during which small errors in the forecast models do not compound. However, a caveat is that though the coarser model will be less sensitive to errors our results also suggest that it may be less accurate in forecasting the true ocean dynamics.

Key Points:

- Wind stress perturbation experiments are conducted in two models of the Argentine Basin with different resolutions
- The predictability of SST and surface DIC is approximately one to two weeks for a 1/12° model
- This can be extended to 45 days in the 1/3° model with a corresponding loss of model fidelity

Supporting Information:

Supporting Information may be found in the online version of this article.

Correspondence to:

S. Swierczek,
stan.swierczek.ctr@nrlssc.navy.mil

Citation:

Swierczek, S., Mazloff, M. R., & Russell, J. L. (2021). Investigating predictability of DIC and SST in the Argentine Basin through wind stress perturbation experiments. *Geophysical Research Letters*, *48*, e2021GL095504. https://doi.org/10.1029/2021GL095504

Received 4 AUG 2021
Accepted 22 OCT 2021

Author Contributions:

Conceptualization: Matthew R. Mazloff, Joellen L. Russell
Formal analysis: Stan Swierczek, Matthew R. Mazloff
Funding acquisition: Joellen L. Russell
Investigation: Stan Swierczek
Methodology: Matthew R. Mazloff
Project Administration: Joellen L. Russell
Software: Stan Swierczek, Matthew R. Mazloff
Supervision: Matthew R. Mazloff, Joellen L. Russell
Validation: Stan Swierczek
Visualization: Stan Swierczek

1. Introduction

The Argentine Basin is a region of the Atlantic sector of the Southern Ocean, bounded to the west by the Patagonian Shelf and to the south by the Malvinas Plateau. Figure 1 shows the bathymetry of the Basin and surrounding area, with the deep basin in dark blue and the shallow areas in white. The collision of two major western boundary currents, the Brazil and Malvinas Currents, occurs in the western edge of the Basin and is the site of the highest mesoscale energy and sea surface height variability in the global oceans (Chelton et al., 1990; Fu et al., 2001). The Brazil-Malvinas Confluence (BMC) features SST gradients exceeding 10°C between the two currents (Tokinaga et al., 2005), warm core eddies >5° C warmer and 1 psu saltier than adjacent waters (de Souza et al., 2006), and cold core eddies similarly cooler and fresher than adjacent waters (Gordon, 1989). Observations of this portion of the Argentine Basin demonstrate a rich vertical structure, with seven distinct water mass layers of both northern and southern origins (Valla et al., 2018). The confluence also drives a powerful stationary barotropic vortex, the Zapiola Anticyclone, over a rise in the center of the Basin (Reid, 2012; Weijer et al., 2020). The location of the BMC is itself variable due to inconsistencies in the Malvinas Current (Artana et al., 2016; Spadone & Provost, 2009) and has been drifting south since 1993 (Combes & Matano, 2014). Large uncertainties surrounding air-sea exchanges of heat (Frölicher et al., 2015) persist due to atmospheric variability (Pezzi et al., 2005) and eddies and meanders that modify surface meteorological variables and modulate the marine atmospheric boundary layer (Souza et al., 2021). There are also large uncertainties surrounding air-sea exchanges of carbon due to poor observational coverage both spatially and seasonally (Gray et al., 2018) and due to the sensitive balance of strong

Writing – original draft: Stan Swierczek
Writing – review & editing: Stan Swierczek, Matthew R. Mazloff, Joellen L. Russell

upwelling of natural carbon from the deep ocean competing with strong uptake of anthropogenic carbon at the surface both occurring in the Basin (Gruber et al., 2009).

As computing power has increased in recent decades, ocean model simulations have increased in resolution from coarse (~1°) to eddy-permitting (~0.25°) to eddy-resolving (~0.1°). However, ocean in situ observational coverage has not kept pace spatially or temporally and high resolution models that utilize data assimilation suffer from decreased predictive skill (Jacobs et al., 2021). Absent assimilation, increasing model resolution in ocean simulations can reduce some biases and introduce others (Chassignet et al., 2020), and the effects of increasing resolution on heat transport, currents, sea level variability, and other quantities has been studied at the global climate level (e.g., Griffies et al., 2015) and also in subregions of interest during shorter time scales (e.g., Ezer & Mellor, 2000; Guo et al., 2003). Predictability can be investigated without hindcasting; the method of perturbing a model with some impulse anomaly and quantifying the response relative to an unperturbed model run has been used extensively in climate studies (Good et al., 2011; Hansen et al., 2011; Hasselmann et al., 1993; Marshall et al., 2017). Predictability of ocean biogeochemical (BGC) variables has been probed using ensemble methods with 1° ocean models (Frölicher et al., 2020; Krumhardt et al., 2020) and estimated through surface wind stress sensitivity experiments (Ridder et al., 2013; Ridder & England, 2014). However, these studies are typically focused on interannual to decadal prediction using coarser climate models and emphasize statistical skill as much as deterministic skill.

Using ensemble methods, Kim et al. (2009) assess the predictability of the coastal ocean off Oregon on shorter time scales in a model with 2 km grid spacing, and find that the deterministic response is stronger than instability growth over the 3–7 days forecast intervals they considered. Investigating loss of predictability by instability growth was similarly investigated for the California Current using perturbation methods by Moore et al. (2009) and Verdy et al. (2014). Moore et al. (2009) found that a tangent linear assumption for a ~20 km resolution model of the region was valid for about 30 days. The wind stress perturbation experiment described in Section 3 of Verdy et al. (2014) provides a template for analyzing regional deterministic predictive capability and we apply this procedure to a model of the Argentine Basin and surrounding area. The choice of a wind stress perturbation has implications for the ocean response. Our interest, however, is not in the exact form of the response, but rather in the growth rate due to nonlinearities. It is this growth that amplifies model errors and limits predictability, and we hypothesize arises equally from errors in momentum or buoyancy fluxes.

Our goal in this paper is to implement techniques from these prior studies and apply them to a general circulation model of the Argentine Basin with biogeochemistry to investigate predictability of physical and BGC variables at the surface via a series of wind stress anomaly perturbation experiments at both eddy-permitting and eddy-resolving resolutions. We want to quantify the time scale of the linear response of sea surface temperature (SST) and surface dissolved inorganic carbon (DIC) at 1/3° and 1/12° horizontal resolutions to determine approximately how long small errors introduced though the atmospheric state at each resolution stay small. Further analysis probes the difference in the response of these models to assess the prospect of forecast skill degradation with coarser resolution models. We choose DIC because it is a primary component of the carbon system and directly related to air-sea carbon fluxes. However, we have repeated the calculations presented with other BGC variables (oxygen, nitrate, net primary production, chlorophyll, and particulate organic carbon) both in the surface cell and the mean of the upper 100 m. The results in all cases are similar and are discussed in Section 3.2.

2. Methods

We construct a regional configuration of the MIT general circulation model [MITgcm, evolved from Adcroft et al. (2011) and Marshall et al. (1997)] with the Nitrogen version of the Biogeochemistry with Light, Iron, Nutrients, and Gases model [N-BLING; evolved from Galbraith et al. (2010)] at two different resolutions. We describe the physical and BGC setup in Section 2.1, the experiment design in Section 2.2, and the method of decomposing the perturbed response into linear and nonlinear signals in Section 2.3.

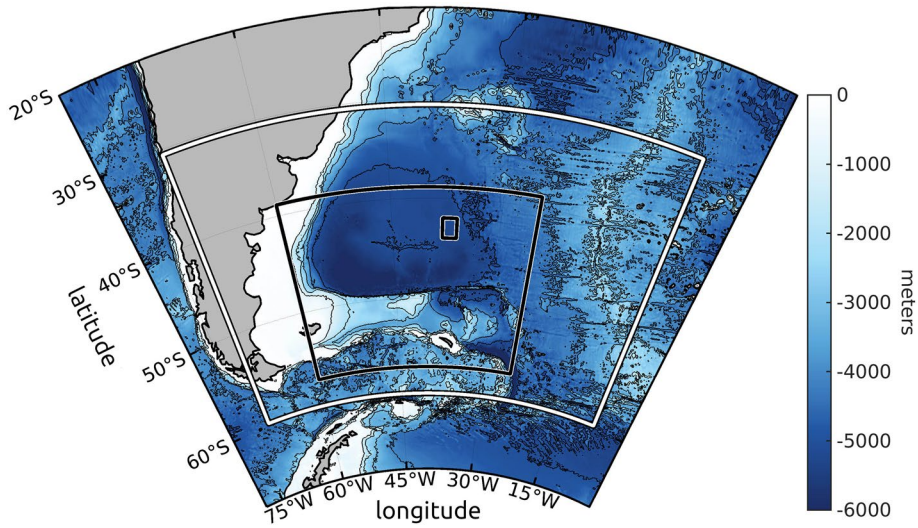

Figure 1. Bathymetry of Argentine Basin and surrounding area with model domain outlined in white, and large and small wind stress anomaly areas outlined in black. 1,000-m contours are shown. The large wind stress anomaly area covers where the Malvinas Current branches off from the Antarctic circumpolar current (ACC) (55° W, 55° S) and the Brazil-Malvinas Confluence (55° W, 38° S), both turbulent areas, while the small perturbation is selected away from those areas.

2.1. Physical and BGC Model Configuration

We use two model configurations, one at 1/3° and another at 1/12° zonal resolution that are identical to those in Swierczek et al. (2021). Meridional spacing is chosen to maintain $\Delta x = \Delta y$. This corresponds to cell widths of 32 km at the northern boundary and 19 km at the southern boundary for the 1/3° model, and 8 and 5 km for the 1/12° respectively. The 1/3° (1/12°) model has 52 (104) vertical levels that vary in height from 4.2 to 400 m (2.1–200 m), with 33 (66) levels in the upper 750 m. The domain extends from 70°W to 8°W and from 60°S to 30°S and includes a 1° /restoring layer along each lateral boundary. Model time-stepping is achieved with a third order Adams-Bashforth scheme that features implicit vertical diffusion and viscosity, a nonlinear free surface, exact volume conservation, and z* time-varying vertical coordinates of Adcroft and Campin (2004). Bathymetry is derived from ETOPO1 (Amante and Eakins, 2009; NOAA National Geophysical Data Center, 2009). We use 30-min time steps in the 1/3° model and 2 min in the 1/12°. Parameterizations of mixed layer and viscosity are implemented using the GGL90 (Gaspar et al., 1990) and modified Leith schemes (Adcroft et al., 2011), respectively.

Open ocean boundary and initial conditions for the two models are provided by the BGC Southern Ocean State Estimate (BSOSE (Verdy & Mazloff, 2017)), a data assimilation ocean–sea ice coupled product that gives a 1/6° solution of the Southern Ocean for the period 2013–2018. We use monthly fields from iteration 122 of BSOSE for lateral forcing of both physical and BGC fields. ERA5 (Copernicus Climate Change Service (C3S), 2017; Hersbach et al., 2020) atmospheric reanalysis provides hourly surface forcing. The Coordinated Ocean-Ice Reference Experiments (CORE) Corrected Normal Year Forcing Version 2.0 datasets (available at https://data1.gfdl.noaa.gov/nomads/forms/core/COREv2/CNYF_v2.html) (Large & Yeager, 2009) give monthly river runoff estimates. Our models do not feature sea ice, tides, or mesoscale eddy parameterizations.

N-BLING (Galbraith et al., 2010) is a BGC model of intermediate complexity for the ocean that is coupled with the MITgcm. Section 2.2 of Verdy and Mazloff (2017) provides a schematic and description for N-BLING. We use atmospheric pCO_2 estimates from the Cape Grim station (obtained from http://www.csiro.au/greenhouse-gases). Both physical and BGC model parameters can be found both in Swierczek et al. (2021) and in the repository reference in the Code Availability section.

2.2. Description of Experiment

We conduct a series of experiments featuring surface wind stress anomalies applied over a small and large area of our model domain. The large area anomaly covers a box from 60°W to 25°W and 57°S to 39°S. The small area anomaly covers a box from 38°W to 36°W and 44°S to 42°S. These wind anomaly areas are plotted in dotted lines in Figure 1 with the model domain outlined in white. The large area anomaly is chosen to hit the ocean with a substantial impulse that covers all unstable regions. The small area anomaly location is chosen to avoid the highly turbulent BMC and determine the sensitivity to a small perturbation in a more stable region.

For each resolution, the models are initialized on December 1, 2016 and run to the end of December for a spinup period and the final state is stored. From this December 31st 2016 model state we run the model five times. The first model run is a control run where we keep the unaltered ERA5 atmospheric forcing. The second features a strengthening of the surface wind stress forcing by 0.1 N/m^2 over the large area one hour after restarting (midday on December 31st) and lasting for one hour. The third model run features a weakening of the surface wind stress by 0.1 N/m^2 over the large area having the same starting time and duration. The fourth and fifth models have the same strengthening and weakening of wind stress as the second and third models but occur over the small area instead. All models are run for four months and diagnostics are recorded every 6 hr. The amplitude of the perturbation is negligible with respect to the regional mesoscale variability. The deterministic response to this perturbation is therefore of little interest. However, the growth of this small response to a non-negligible size is of primary interest with regards to limiting predictability, as we hypothesize that this is a reasonable amplitude perturbation that may arise from errors in the model inputs and numerics.

2.3. Method of Decomposition Into Linear and Nonlinear Response

We analyze our model output using the technique described in Section 3 of Verdy et al. (2014). We define h_0 to be the SST or surface DIC of the control run, h_+ to be the corresponding field during the positive wind stress anomaly run, and h_- to be the field from the negative wind stress anomaly run. We calculate the differences between the positive anomaly and the control, $\delta h_1 = h_+ - h_0$, and between the negative anomaly and the control, $\delta h_2 = h_- - h_0$ for each of SST and DIC. Decomposing the perturbed runs as Taylor expansions around the control run, we can isolate the odd order terms by computing $\delta H_1 = \frac{1}{2}(\delta h_1 - \delta h_2)$ and the even terms with $\delta H_2 = \frac{1}{2}(\delta h_1 + \delta h_2)$. We can consider δH_1 the linear response as long as δH_2 is approximately one order of magnitude smaller than δH_1. δH_2 can be considered the nonlinear response in this case as the quadratic term is the first nonlinear term of the Taylor expansion. We will use the terms linear and nonlinear in describing the response even though this is approximately true only under this condition. We analyze the results both by looking directly at δH_1 and δH_2 as in Figures 2 and 3, and by taking the root mean square (RMS) magnitude of δH_1 and δH_2 averaged over the model domain minus the sponge layer as in Figure 4. When the response is dominated by the linear term and decaying, we consider the model to be "predictable."

3. Results of Perturbation Experiments

3.1. Snapshots of Linear and Nonlinear Responses

Snapshots of 1, 10, 20, 30, and 40 days surface DIC responses to the large wind anomaly are shown in Figure 2. The extent of the wind anomaly is clearly visible in the 1 day snapshots. The 1/3° and 1/12° models one day linear responses show noticeable effects over the whole perturbation area and also outside the area along the South American coast north of the box, west of the Brazil Current. The linear responses of the 1/3° model looks like a smoothed version of the 1/12° model linear response at 1 day and at 10 days. By 30 and 40 days, however, the 1/3° model linear response has mostly decayed away while the higher order odd terms of the 1/12° have grown enough in the BMC and also at the southern boundary. The nonlinear response for the 1/3° model decays away by 10 days enough to be barely visible at the plot color scale save for a few spots. The 1/12° model nonlinear response is small by 10 days, mostly appearing in the BMC and at three eddies. Progressing from 20 to 40 days, the responses around the BMC and at the northeast of the domain are the most notable.

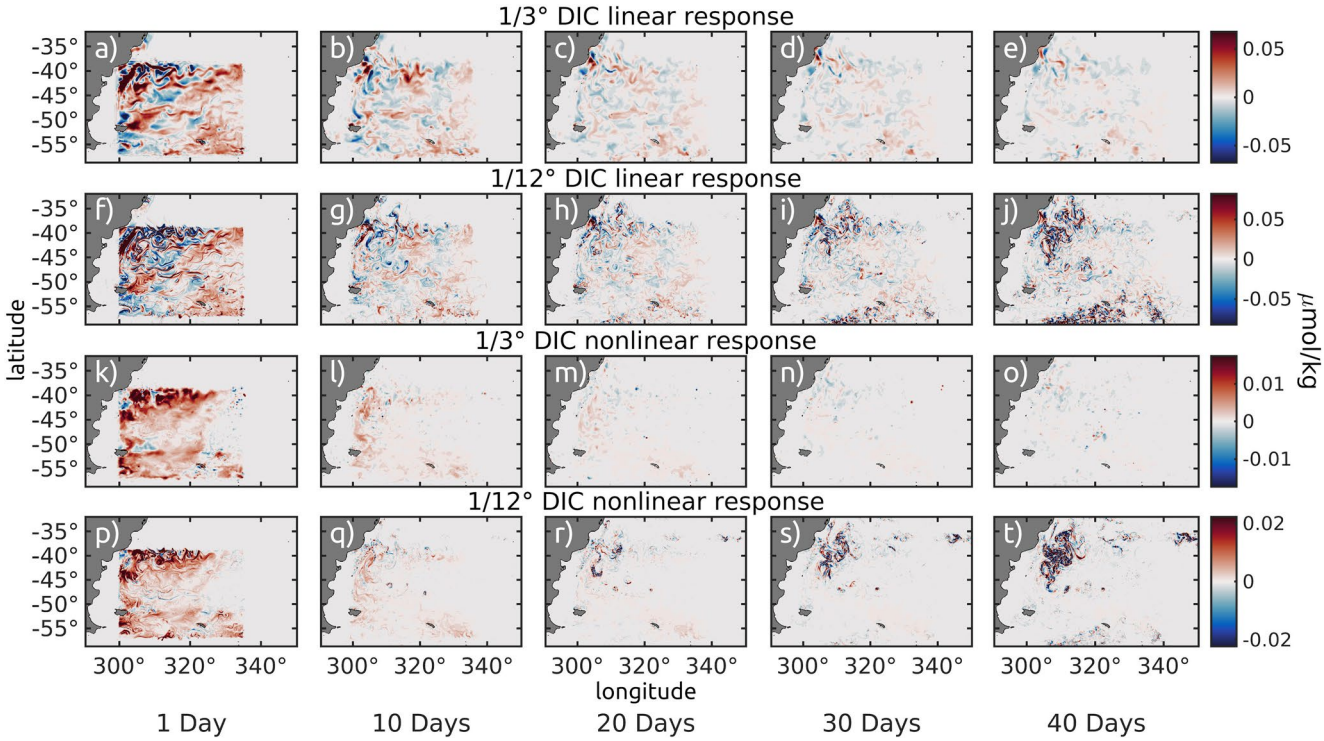

Figure 2. The linear and nonlinear surface DIC responses to the large area perturbation. Columns represent snapshots of 1, 10, 20, 30, and 40 days responses. The rows show 1/3° model linear, 1/12° linear, 1/3° nonlinear, and 1/12° nonlinear responses respectively. The 1/3° model linear response again shows smooth features that decay in magnitude after the wind stress perturbation. The 1/12° model linear and nonlinear response both feature major instabilities triggered by the 20 days mark. Note the color scales are slightly different so the responses are visible in each row.

We next discuss the small area perturbation experimental results. Figure 3 shows snapshots of δH_1 and δH_2 for surface DIC at 1, 10, 20, 30, and 40 days after the wind anomaly for both resolutions. δH_1 can be considered the linear response up to approximately 45 days in the 1/3° model and 15 days in the 1/12°. The 1 day responses for both resolutions are largely confined to the location of the wind anomaly. The linear response of the 1/3° model looks like a smoothed 1/12° linear response for the 10 days snapshot and the 20 days to a lesser extent, but by 30 days the higher order odd terms begin to dominate the linear term in the 1/12°. Thus the 30 and 40 days snapshots in the 1/12° are no longer 'linear' in the second row of panels (this will be discussed in Figure 4). We see instabilities growing in the BMC away from the anomaly location, and also three anomalies along the center of the domain that are not resolved in the 1/3° model. The linear and nonlinear responses in the 1/12° model appear in these eddies by the 10th day.

The 1/3° model nonlinear response does not have areas of magnitude notable enough at the chosen color scale after the first day, except for a few spots at 40 days. The 1/12° model nonlinear response appears over the wind anomaly one day after, but by 10 days is visible at the three eddies and near the BMC by 20 days. By 30 and 40 days, there are massive areas with sharp and complicated positive and negative responses mostly centered around the BMC.

Figures S1 and S2 in Supporting Information S1 show the same snapshots for SST. The spatiotemporal evolution of linear and nonlinear responses for SST are largely the same as for surface DIC. The opposite vertical gradients of temperature and carbon cause the signs of the responses to be flipped; subsurface waters have lower temperatures but are more carbon-rich so increased mixing, for example, will show opposite colors in the corresponding plots.

3.2. RMS Magnitude of Response and Skill

We calculate the RMS magnitudes of δH_1 and δH_2 for SST and surface DIC for every 6 hr through the model runs. The calculation is performed over the interior of the model domain inside of the sponge layer and the

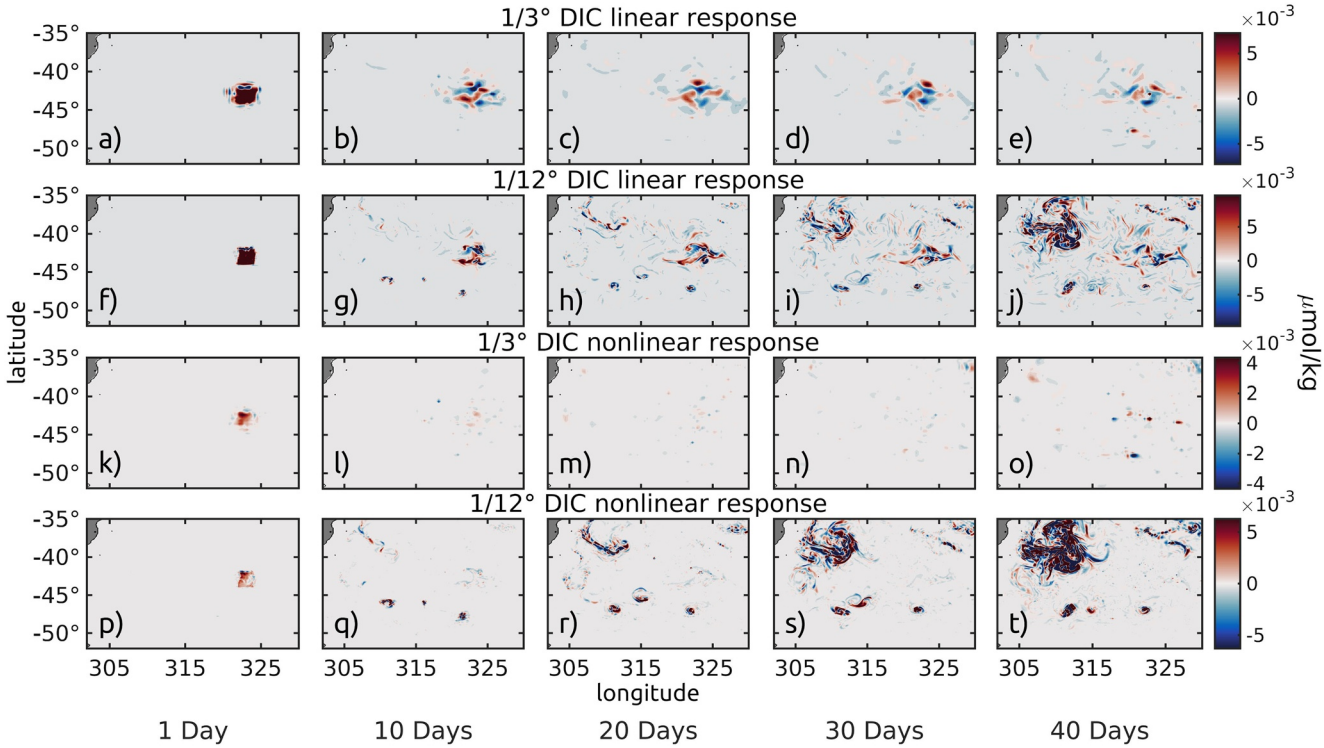

Figure 3. The linear and nonlinear surface DIC responses to the small area perturbation. Columns represent snapshots of 1, 10, 20, 30, and 40 days responses. The rows show 1/3° model linear, 1/12° linear, 1/3° nonlinear, and 1/12° nonlinear responses, respectively. The 1/3° model linear response shows smooth features that decay in magnitude after the initial shock but remain local to the wind anomaly. The 1/12° model linear and nonlinear responses both show sharper features after several weeks that possibly indicate changes in front locations resulting from the wind anomaly. Note the color scales are slightly different so the responses are visible in each row.

results are shown in Figure 4. The solid lines show δH_1 and the dotted lines show δH_2. When δH_1 is an order of magnitude larger than δH_2 for each corresponding field and resolution, and is decreasing in magnitude, δH_1 is interpretable as the linear response. We look for how many days the responses are decaying to approximately determine predictability. The RMS for the large anomaly model runs are larger than the RMS for the small. More notably, the RMS stops decaying and begins increasing sooner in the small anomaly model runs than in the large. The linear responses for SST and DIC decay for as long as 48 days in the 1/3° model and 17 days in the 1/12° model for the large wind anomaly model runs. This is reduced to 33 and 9 days, respectively, in the small anomaly model runs. This suggests that this domain is naturally unstable in most regions and that errors will grow eventually no matter where the model is perturbed, although we only have tried one area for the small perturbation experiment.

Table S1 in Supporting Information S1 details the duration of the decay of the responses. It is worth noting that the RMS linear response of the 1/12° model SST and DIC to the small perturbation stops decaying at 9 days but it does not begin to substantially increase until approximately 30 days, and is still larger than the nonlinear response for at least 15 days.

The 1/3° model is less sensitive to perturbations (e.g., from model input errors) and may be useful for extended duration forecasting, but we must evaluate the realism of the 1/3° model response. Here we consider the 1/12° model to be the "real ocean" as it resolves more of the physical scales. Our definition of skill is in terms of the proportion of variance explained and is calculated following Goddard et al. (2013) and also described here. We define SST^+ as SST (positive perturbation run) – SST (control run). At each time step, we calculate the spatial variance (var) of the 1/12° SST^+ field and of the difference 1/12° SST^+ – 1/3° SST^+. The skill is then $1 - \mathrm{var}(1/12^\circ - 1/3^\circ\ SST^+)/(\mathrm{var}(1/12^\circ\ SST^+)$. Importantly, before we perform this calculation we apply a 1/2° (roughly 40 km) Gaussian filter to smooth both the 1/3° and the 1/12° model SST^+ fields because our primary goal is to evaluate how well the 1/3° model can forecast the large scale structures of

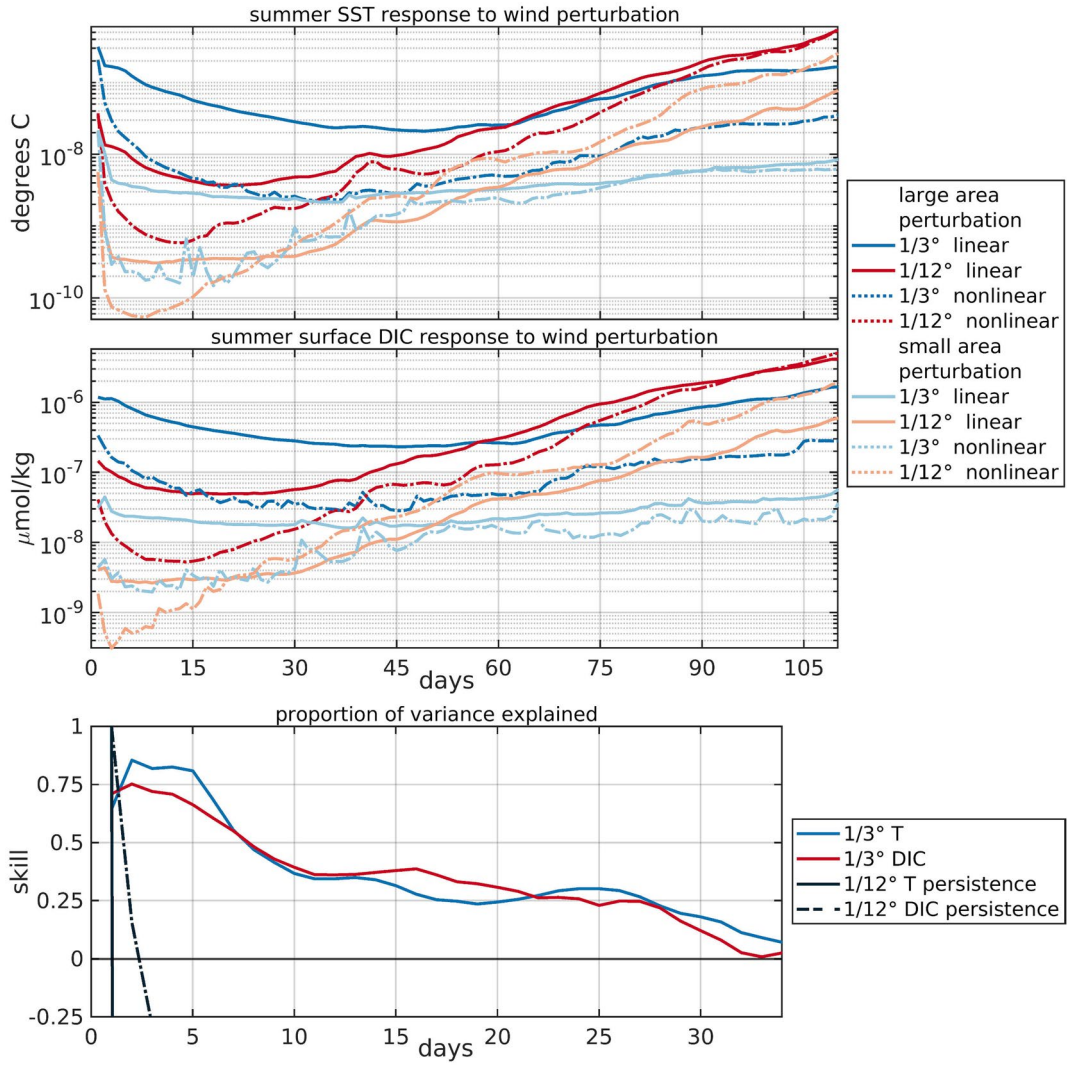

Figure 4. The root mean square (RMS) magnitude of the summer (a) SST and (b) surface DIC responses to the large and small wind anomalies plotted against time. The bold colors show the large area responses and the pale colors show the small area responses. The blue colors represent the 1/3° models and the red represent the 1/3° models. The 1/3° models' response decays for longer times than the 1/12° models for both experiments. While the RMS is smaller for the small area wind anomaly response, that RMS stops decaying and begins to increase sooner than the response of the large area anomaly response. (c) Forecast skill of the 1/3° model with respect to the 1/12° model. The 1/3° model is able to account for at least 50% of the variance for about 8 days.

the "real ocean." Figure 4c shows the results of this calculation, and suggests the 1/3° model can explain at least 50% of the variance of the 'real ocean' for about 8 days. We include the skill of the initial 1/12° state used as a persistence forecast.

We perform the same RMS and skill calculations and create additional plots (all in Supporting Information S1) for different combinations of variables and seasons. Surface T and DIC for winter (Figures S4 in Supporting Information S1), upper 100 m T and DIC for summer (Figure S3 in Supporting Information S1) and winter (Figure S5 in Supporting Information S1), surface dissolved oxygen (DO) and chlorophyll for summer (Figure S6 in Supporting Information S1) and winter (Figure S8 in Supporting Information S1), and upper 100 m DO and chlorophyll for summer (Figure S7 in Supporting Information S1) and winter (Figure S9 in Supporting Information S1) are included. Based on these plots, we can conclude the following: (a) T, DIC, DO, and chlorophyll are more sensitive to wind stress perturbations at the surface in summer than in winter (see Figure 4, and S4, S6, and S8 in Supporting Information S1). In summer each responds

with an initial RMS that decays for a period of time before increasing. In winter, the initial magnitude of the responses are smaller but the magnitudes do not decay. (b) The analysis of upper 100 m averages reveals smaller initial responses, and smoother evolution of the responses, but they are not markedly different from the surface quantities. (c) The growth rate of the magnitudes of each quantity are consistent across season and choice of surface or upper 100 m average.

3.3. Conclusion of Experiment

The summer experiment concludes on May 1, 2017. We calculate the difference between the control runs and the perturbation runs on the final time step for each perturbation and each resolution. The results are shown in Figures S10 and S11 in Supporting Information S1 and corroborate the results in Figures 2–4. For both SST and surface DIC, the scale of the differences between the solutions is approximately 1 to 2 orders of magnitude larger in the 1/12° model than in the 1/3°. The locations of the largest effects are different between resolutions. In the 1/3° model, the major differences are at the ACC-Malvinas split and the eastern extent of the Zapiola Anticyclone. In the 1/12° model, the major differences are at the BMC and over the Argentine Abyssal Plain where the highest eddy activity occurs.

4. Summary

In this study, we investigate the response of surface temperature and carbon to wind stress perturbations for models of the Argentine Basin and surrounding areas at two resolutions. We decompose this response into linear and nonlinear terms, and quantify the length of time that these responses decay. This provides a rough estimate for the maximum forecast horizon in this particular area in two circumstances, depending on what physical scales need to be resolved. Due to computational expense, we only perform these experiments once in summer and winter. Future work may involve using an ensemble of experiments or probing different small areas around the domain with the wind stress anomaly in order to determine the sensitivity of these results to the background state.

It is determined that at least for SST and surface DIC, "small" errors (in our case small due to the short duration of the perturbation) in the atmospheric state or initial conditions even over energetic subregions will remain small for $\sim 30 - 45$ days in an eddy-permitting 1/3° model. In an eddy-resolving 1/12° model, this is shortened to $\sim 7 - 14$ days. The spatial locations of the greatest nonlinear responses indicate that the areas of increased eddy activity in the eddy-resolving 1/12° model will be the first to exhibit degraded forecast skill under surface wind stress anomaly errors. The results suggest that the 1/3° model is able to forecast for long periods where small errors in the surface forcings will be damped. However, if we consider the 1/12° model as a stand-in for the real ocean, it is also important for the 1/3° model to give a solution that looks like a smoothed version of the 1/12° model solution. Figure 4 and S3–S9 in Supporting Information S1 all show this is only true for about one week. We conclude that the 1/3° model has long predictability, but lacks in deterministic skill at lead times greater than approximately one week. Meanwhile, our results suggest an eddy resolving model of this most energetic and turbulent ocean region has predictability for lead times out to two weeks. We therefore hypothesize that two weeks is a lower bound for duration of ocean surface property predictability at the mesoscale more generally across the globe.

Data Availability Statement

The Biogeochemical Southern Ocean State Estimate fields used for initialization and forcing are from http://sose.ucsd.edu/BSOSE6_iter122_solution.html. The ERA5 reanalysis is available at https://www.ecmwf.int/en/forecasts/datasets/reanalysis-datasets/era5. The codes to run the regional models in the paper are publicly available in the following repository: https://doi.org/10.5281/zenodo.5576905. The latest version of the MITgcm is available at https://doi.org/10.5281/zenodo.4968496.

Acknowledgments
This work was sponsored by NSF's Southern Ocean Carbon and Climate Observations and Modeling (SOCCOM) Project under the NSF award PLR-1425989. All of the data used in this analysis is available online. The source of the Cape Grim atmospheric CO_2 is CSIRO Oceans & Atmosphere and the Australian Bureau of Meteorology (Cape Grim Baseline Air Pollution Station). CSIRO and the Australian Bureau of Meteorology give no warranty regarding the accuracy, completeness, currency, or suitability for any particular purpose and accept no liability in respect of data.

References

Adcroft, A., & Campin, J.-M. (2004). Rescaled height coordinates for accurate representation of free-surface flows in ocean circulation models. *Ocean Modelling*, *7*(3), 269–284. https://doi.org/10.1016/j.ocemod.2003.09.003

Adcroft, A., Dutkiewicz, S., Ferreira, D., Heimbach, P., Jahn, O., & Maze, G. (2011). *MITgcm user manual [Computer software manual]*. Retrieved from http://mitgcm.org/public/r2_manual/latest/online_documents/manual.pdf

Amante, C., & Eakins, B. W. (2009). *ETOPO1 1 arc-minute global relief model: Procedures, data sources and analysis. NOAA technical memorandum NESDIS NGDC–24*. Computer software manual. National Geophysical Data Center, NOAA. https://doi.org/10.7289/V5C8276M

Artana, C., Ferrari, R., Koenig, Z., Saraceno, M., Piola, A. R., & Provost, C. (2016). Malvinas current variability from Argo floats and satellite altimetry. *Journal of Geophysical Research: Oceans*, *121*(7), 4854–4872. https://doi.org/10.1002/2016jc011889

Chassignet, E. P., Yeager, S. G., Fox-Kemper, B., Bozec, A., Castruccio, F., Danabasoglu, G., et al. (2020). Impact of horizontal resolution on global ocean–sea ice model simulations based on the experimental protocols of the ocean model intercomparison project phase 2 (OMIP-2). *Geoscientific Model Development*, *13*(9), 4595–4637. https://doi.org/10.5194/gmd-13-4595-2020

Chelton, D. B., Schlax, M. G., Witter, D. L., & Richman, J. G. (1990). Geosat altimeter observations of the surface circulation of the Southern Ocean. *Journal of Geophysical Research: Oceans*, *95*(C10), 17877–17903. https://doi.org/10.1029/JC095ic10p17877

Combes, V., & Matano, R. P. (2014). Trends in the Brazil/Malvinas confluence region. *Geophysical Research Letters*, *41*(24), 8971–8977. https://doi.org/10.1002/2014gl062523

Copernicus Climate Change Service (C3S). (2017). *ERA5: Fifth generation of ECMWF atmospheric reanalyses of the global climate Copernicus climate change Service climate data Store (CDS)*. 2020–04–19. Retrieved from https://cds.climate.copernicus.eu/cdsapp//#!/home

de Souza, R. B., Mata, M. M., Garcia, C. A., Kampel, M., Oliveira, E. N., & Lorenzzetti, J. A. (2006). Multi-sensor satellite and in situ measurements of a warm core ocean eddy south of the Brazil–Malvinas Confluence region. *Remote Sensing of Environment*, *100*(1), 52–66. https://doi.org/10.1016/j.rse.2005.09.018

Ezer, T., & Mellor, G. L. (2000). Sensitivity studies with the North Atlantic sigma coordinate princeton ocean model. *Dynamics of Atmospheres and Oceans*, *32*(3), 185–208. https://doi.org/10.1016/s0377-0265(00)00047-6

Frölicher, T. L., Ramseyer, L., Raible, C. C., Rodgers, K. B., & Dunne, J. (2020). Potential predictability of marine ecosystem drivers. *Biogeosciences*, *17*(7), 2061–2083. https://doi.org/10.5194/bg-17-2061-2020

Frölicher, T. L., Sarmiento, J. L., Paynter, D. J., Dunne, J. P., Krasting, J. P., & Winton, M. (2015). Dominance of the Southern Ocean in anthropogenic carbon and heat uptake in CMIP5 models. *Journal of Climate*, *28*(2), 862–886. https://doi.org/10.1175/JCLI-D-14-00117.1

Fu, L.-L., Cheng, B., & Qiu, B. (2001). 25-day period large-scale oscillations in the Argentine Basin revealed by the TOPEX/Poseidon altimeter. *Journal of Physical Oceanography*, *31*(2), 506–517. https://doi.org/10.1175/1520-0485(2001)031⟨0506:DPLSOI⟩2.0.CO;2

Galbraith, E., Gnanadesikan, A., Dunne, J., & Hiscock, M. R. (2010). Regional impacts of iron-light colimitation in a global biogeochemical model. *Biogeosciences*, *7*(3), 1043–1064. https://doi.org/10.5194/bg-7-1043-2010

Gaspar, P., Grégoris, Y., & Lefevre, J.-M. (1990). A simple eddy kinetic energy model for simulations of the oceanic vertical mixing: Tests at station Papa and long-term upper ocean study site. *Journal of Geophysical Research: Oceans*, *95*(C9), 16179–16193. https://doi.org/10.1029/jc095ic09p16179

Goddard, L., Kumar, A., Solomon, A., Smith, D., Boer, G., Gonzalez, P., et al. (2013). A verification framework for interannual-to-decadal predictions experiments. *Climate Dynamics*, *40*(1), 245–272. https://doi.org/10.1007/s00382-012-1481-2

Good, P., Gregory, J. M., & Lowe, J. A. (2011). A step-response simple climate model to reconstruct and interpret AOGCM projections. *Geophysical Research Letters*, *38*(1), L01703. https://doi.org/10.1029/2010gl045208

Gordon, A. L. (1989). Brazil-Malvinas Confluence–1984.*Deep Sea Research Part I: Oceanographic Research Papers*, *36*(3), 359–384. https://doi.org/10.1016/0198-0149(89)90042-3

Gray, A. R., Johnson, K. S., Bushinsky, S. M., Riser, S. C., Russell, J. L., Talley, L. D., et al. (2018). Autonomous biogeochemical floats detect significant carbon dioxide outgassing in the high-latitude Southern Ocean. *Geophysical Research Letters*, *45*(17), 9049–9057. https://doi.org/10.1029/2018gl078013

Griffies, S. M., Winton, M., Anderson, W. G., Benson, R., Delworth, T. L., Dufour, C. O., et al. (2015). Impacts on ocean heat from transient mesoscale eddies in a hierarchy of climate models. *Journal of Climate*, *28*(3), 952–977. https://doi.org/10.1175/JCLI-D-14-00353.1

Gruber, N., Gloor, M., Mikaloff Fletcher, S. E., Doney, S. C., Dutkiewicz, S., Follows, M. J., & Takahashi, T. (2009). Oceanic sources, sinks, and transport of atmospheric CO_2. *Global Biogeochemical Cycles*, *23*(1), GB1005. https://doi.org/10.1029/2008gb003349

Guo, X., Hukuda, H., Miyazawa, Y., & Yamagata, T. (2003). A triply nested ocean model for simulating the Kuroshio—Roles of horizontal resolution on JEBAR. *Journal of Physical Oceanography*, *33*(1), 146–169. https://doi.org/10.1175/1520-0485(2003)033⟨0146:ATNOMF⟩2.0.CO;2

Hansen, J., Sato, M., Kharecha, P., & von Schuckmann, K. (2011). Earth's energy imbalance and implications. *Atmospheric Chemistry and Physics*, *11*(24), 13421–13449. https://doi.org/10.5194/acp-11-13421-2011

Hasselmann, K., Sausen, R., Maier-Reimer, E., & Voss, R. (1993). On the cold start problem in transient simulations with coupled atmosphere-ocean models. *Climate Dynamics*, *9*(2), 53–61. https://doi.org/10.1007/BF00210008

Hersbach, H., Bell, B., Berrisford, P., Hirahara, S., Horányi, A., Muñoz-Sabater, J., et al. (2020). The ERA5 global reanalysis. *Quarterly Journal of the Royal Meteorological Society*, *146*, 1999–2049. https://doi.org/10.1002/qj.3803

Jacobs, G., D'Addezio, J. M., Ngodock, H., & Souopgui, I. (2021). Observation and model resolution implications to ocean prediction. *Ocean Modelling*, *159*, 101760. https://doi.org/10.1016/j.ocemod.2021.101760

Kim, S., Samelson, R. M., & Snyder, C. (2009). Ensemble-based estimates of the predictability of wind-driven coastal ocean flow over topography. *Monthly Weather Review*, *137*(8), 2515–2537. https://doi.org/10.1175/2009mwr2631.1

Krumhardt, K. M., Lovenduski, N. S., Long, M. C., Luo, J. Y., Lindsay, K., Yeager, S., & Harrison, C. (2020). Potential predictability of net primary production in the ocean. *Global Biogeochemical Cycles*, *34*(6), 1–14. https://doi.org/10.1029/2020GB006531

Large, W. G., & Yeager, S. G. (2009). The global climatology of an interannually varying air–sea flux data set. *Climate Dynamics*, *33*(2), 341–364. https://doi.org/10.1007/s00382-008-0441-3

Marshall, J., Adcroft, A., Hill, C., Perelman, L., & Heisey, C. (1997). A finite-volume, incompressible Navier Stokes model for studies of the ocean on parallel computers. *Journal of Geophysical Research*, *102*(C3), 5753–5766. https://doi.org/10.1029/96jc02775

Marshall, J., Scott, J., & Proshutinsky, A. (2017). "Climate response functions" for the Arctic Ocean: A proposed coordinated modelling experiment. *Geoscientific Model Development*, *10*(7), 2833–2848. https://doi.org/10.5194/gmd-10-2833-2017

Moore, A. M., Arango, H. G., Lorenzo, E. D., Miller, A. J., & Cornuelle, B. D. (2009). An adjoint sensitivity analysis of the Southern California Current circulation and ecosystem. *Journal of Physical Oceanography*, *39*(3), 702–720. https://doi.org/10.1175/2008jpo3740.1

NOAA National Geophysical Data Center. (2009). *ETOPO1 1 arc-minute global relief model*. National Centers for Environmental Information. (Accessed [2019–02–01]).

Pezzi, L. P., Souza, R. B., Dourado, M. S., Garcia, C. A. E., Mata, M. M., & Silva-Dias, M. A. F. (2005). Ocean-atmosphere in situ observations at the Brazil-Malvinas Confluence region. *Geophysical Research Letters*, *32*(22), L22603. https://doi.org/10.1029/2005gl023866

Reid, J. (2012). Deep circulation within the Argentine Basin. *Journal of Marine Research*, *70*, 199–203. https://doi.org/10.1357/002224012800502354

Ridder, N. N., & England, M. H. (2014). Sensitivity of ocean oxygenation to variations in tropical zonal wind stress magnitude. *Global Biogeochemical Cycles*, *28*(9), 909–926. https://doi.org/10.1002/2013gb004708

Ridder, N. N., Meissner, K. J., & England, M. H. (2013). Sensitivity of the oceanic carbon reservoir to tropical surface wind stress variations. *Geophysical Research Letters*, *40*(10), 2218–2223. https://doi.org/10.1002/grl.50498

Souza, R., Pezzi, L., Swart, S., Oliveira, F., & Santini, M. (2021). Air-sea interactions over eddies in the Brazil-Malvinas confluence. *Remote Sensing*, *13*(7). https://doi.org/10.3390/rs13071335

Spadone, A., & Provost, C. (2009). Variations in the Malvinas Current volume transport since October 1992. *Journal of Geophysical Research*, *114*(C2), C02002. https://doi.org/10.1029/2008jc004882

Swierczek, S., Mazloff, M. R., Morzfeld, M., & Russell, J. L. (2021). The effect of resolution on vertical heat and carbon transports in a regional ocean circulation model of the Argentine Basin. *Journal of Geophysical Research: Oceans*, *126*(7), e2021JC017235. https://doi.org/10.1029/2021JC017235

Tokinaga, H., Tanimoto, Y., & Xie, S.-P. (2005). SST-induced surface wind variations over the Brazil–Malvinas Confluence: Satellite and in situ observations. *Journal of Climate*, *18*(17), 3470–3482. https://doi.org/10.1175/jcli3485.1

Valla, D., Piola, A. R., Meinen, C. S., & Campos, E. (2018). Strong mixing and recirculation in the northwestern Argentine Basin. *Journal of Geophysical Research: Oceans*, *123*(7), 4624–4648. https://doi.org/10.1029/2018jc013907

Verdy, A., & Mazloff, M. R. (2017). A data assimilating model for estimating southern ocean biogeochemistry. *Journal of Geophysical Research: Oceans*, *122*(9), 6968–6988. https://doi.org/10.1002/2016jc012650

Verdy, A., Mazloff, M. R., Cornuelle, B. D., & Kim, S. Y. (2014). Wind-driven sea level variability on the California Coast: An adjoint sensitivity analysis. *Journal of Physical Oceanography*, *44*(1), 297–318. https://doi.org/10.1175/jpo-d-13-018.1

Weijer, W., Barthel, A., Veneziani, M., & Steiner, H. (2020). The Zapiola anticyclone: A Lagrangian study of its kinematics in an eddy-permitting ocean model. *Deep Sea Research Part I: Oceanographic Research Papers*, *164*, 103308. https://doi.org/10.1016/j.dsr.2020.103308